Borohydride Hydrolysis Using a Mechanically and Chemically Stable Aluminium-Stainless Steel Porous Monolith Catalyst Made by 3D Printing

Pope, F.; Xhaferri, X.; Giesen, D.; Geels, N.J.; Pichler, J.; Rothenberg, G.

DOI
10.1002/cssc.202401264

Publication date
2025

Document Version
Final published version

Published in
ChemSusChem

ChemSusChem

Research Article
doi.org/10.1002/cssc.202401264

Chemistry Europe
European Chemical Societies Publishing

www.chemsuschem.org

Borohydride Hydrolysis Using a Mechanically and Chemically Stable Aluminium-Stainless Steel Porous Monolith Catalyst Made by 3D Printing

Frances Pope,[a] Xhoi Xhaferri,[a] Daan Giesen,[b] Norbert J. Geels,[a] Jessica Pichler,[c] and Gadi Rothenberg*[a]

The challenge of moving to a carbon-free energy economy is highlighted in the context of technology and materials restrictions. Many technologies needed for the so-called energy transition depend on critical metals such as platinum, lithium, iridium and cobalt. Here we focus on solid borohydride salts as hydrogen carriers, studying catalysts for hydrogen release. We combine metal 3D printing technology and a Raney-type leaching process to make structured macroscopic catalyst/reactor monoliths of cobalt, aluminium and stainless steel with well-defined micropores. Remarkably, the blank catalyst samples, which are made only from aluminium and stainless steel (Al-SS), show high activity and, importantly, high stability in borohydride hydrolysis, with no mass loss and no surface poisoning. The batch results are confirmed in a continuous setup running for 96 h. Catalyst performance is attributed to the stable porous structure, the mechanical stability of the stainless steel macrostructure, and the presence of accessible Al(OH)x sites. This research shows a clear contribution to sustainability based on multi-factor comparison: The Al-SS catalyst outperforms the state-of-the-art on mechanical and chemical durability, it is both PGM-free and CRM-free, and its preparation follows a simple, scalable and low-waste procedure.

Introduction

Time is running out. To minimise the climate crisis, our world must undergo a large and profound transition, from carbon-based energy to carbon-free energy, by 2050.[1,2] Most of the *science* needed for this transition is available, at least in theory. Yet actual large-scale application is challenging, not least because many of the *technologies* needed are still unoptimized and depend on rare and expensive elements.[3] A further confounding factor is that many of these are located in specific countries: Platinum in South Africa, Lithium in Bolivia and Argentina, Cobalt in Congo and Australia, and rare-earths in China.[4–7] Transporting these materials already increases their carbon footprint.[8] Thus, a sustainable society should aim at technologies based on abundant and local materials, that can operate continuously with long cycle times.

Our goal is moving to hydrogen-based energy carriers. The reason is simple: Burning carbon, in whatever form, ultimately emits CO_2, while burning hydrogen gives only water. The switch to using hydrogen as an energy carrier is likely to be gradual, starting from a combination of "grey", "blue" and "green" hydrogen, and ending (hopefully) with the latter as the main variant.[9]

Yet using molecular hydrogen as an energy carrier on a large scale has its drawbacks, especially in applications requiring storage and transport. One way to overcome these is using solid hydrides, such as borohydride salts. These salts enable safe and efficient transportation of hydrogen in hydride form, and therefore suitable for mobile applications such as trucks, boats and mobile generators. The hydrogen can be released from the salt by a reacting with water in the presence of a catalyst (Equation (1)). There are two problems, however. The first is that the best catalysts for this reaction are typically noble metals or cobalt, all of which are on the critical raw materials (CRM) list. The second is that even with those catalysts, the reaction can run into long-term problems, with catalyst degradation through hydrogen bubble formation and inhibition/poisoning by the metaborate by-product.[10–13]

$$MBH_4 + (2+x)H_2O \longrightarrow 4\,H_2 + MBO_2 \cdot xH_2O \quad (1)$$

Previously, we showed that encapsulating cobalt in chitosan spheres can lower catalyst decomposition by letting the hydrogen escape through the flexible sphere walls.[14] More recently, we showed that cobalt microparticles can be embedded in stainless steel reactor monoliths using 3D printing, providing a metal support for long-term catalyst durability.[15] However,

[a] *Van 't Hoff Institute for Molecular Sciences, University of Amsterdam, Amsterdam, The Netherlands*
[b] *Technology Centre FNWI, University of Amsterdam, Amsterdam, The Netherlands*
[c] *Austrian Centre of Competence for Tribology, AC2T Research GmbH, Wiener Neustadt, Austria*

Correspondence: *Gadi Rothenberg, Van 't Hoff Institute for Molecular Sciences, University of Amsterdam, Science Park 904, 1098 XH Amsterdam, The Netherlands.*
Email: g.rothenberg@uva.nl

Supporting Information for this article is available on the WWW under https://doi.org/10.1002/cssc.202401264

both catalysts still use cobalt, a critical raw material, as their active site.

As part of the catalyst optimisation process, we ran several protocols intended to increase the monoliths' porosity inspired by Raney's method.[16] Surprisingly, we discovered that our cobalt-free control was highly active and stable, in both batch and continuous systems. Thus, we accidentally synthesised an active catalyst made of only stainless steel and aluminium, both fully recyclable and readily available materials. In this work, we report and discuss the synthesis of these porous macrostructures, as well as their long term activity and durability in potassium borohydride hydrolysis. We compare this to previous work, showing the increase in activity and durability. Finally, we discuss the contributions of this CRM-free catalyst to sustainability in the context of the energy transition.

Results and Discussion

A detailed description of the equipment and concept for 3D printing of the catalytic reactor monolith inserts using selective laser melting (SLM) is published elsewhere.[15] For making porous monoliths, we prepared a metal powder mixture containing 20 wt% Al and 80 wt% stainless steel (SS). This was printed and alloyed in the form of cylindrical monoliths, 12 mm in diameter and 10 mm high, with hexagonal channels 2 mm wide (Figure 1). The printing parameters were tuned to improve the embedding of the aluminium particles in the stainless steel (see experimental section and SI for details).[17] The monoliths were first washed in a mixture of nitric and sulfuric acid. We then leached out part of the aluminium using a 7 M NaOH solution (Equations (2)–(4)), creating a porous structure aluminium-stainless steel structure (herein: Al-SS).[18] The acid prewash corrodes the surface, promoting the leaching of Al^0.

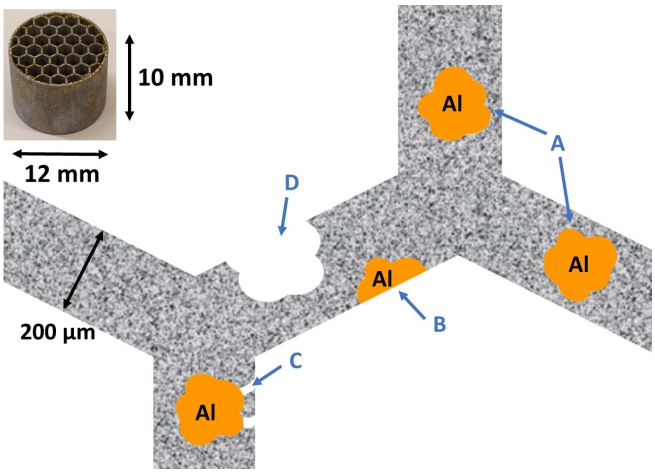

Figure 1. Schematic showing the different types of aluminium sites obtained via metal 3D printing. **A** shows Al particles fully embedded within the walls of the monolith. **B** shows Al exposed and accessible at the monolith channel wall edge. **C** shows porous pathways connecting embedded aluminium to the surface of the monolith. **D** shows the introduction of porosity by removal of an aluminium particle. Inset shows a typical 3d-printed monolith used in this work, the hexagonal channel walls are 200 microns thick.

$$2Al + 6H_2O + 2NaOH \longrightarrow 2NaAl(OH)_4 + 3H_2 \quad (2)$$

$$NaAl(OH)_4 \longrightarrow NaOH + Al(OH)_3 \quad (3)$$

$$2Al + 6H_2O \longrightarrow 2Al(OH)_3 + 3H_2 \quad (4)$$

The preparation of Raney metals typically requires pulverising, because leaching aluminium from macroscopic objects is difficult. The monoliths' small surface area is both uniform and low-energy, resulting in a large kinetic barrier. Using only the base treatment gave <1% leaching. Adding an acid prewashing step corrodes the surface and increases the chance of leaching, while still keeping the structure's mechanical stability. We tested different combinations of acids and pre-wash regimes. Organic acids were reported to dissolve aluminium in clay materials.[19] However, using oxalic acid had no effect, even at 85 °C. Conversely, sulfuric acid gave a highly exothermic reaction with Al at room temperature. Adding a small volume of diluted nitric acid increased the corrosion. The optimal pretreatment for our Al-SS monoliths was using a 60:5:35 wt% H_2SO_4:HNO_3:H_2O solution for 16 h at room temperature (longer durations did not improve the result). The monoliths were then leached using a 7 M NaOH solution at 90 °C for an additional 16 h, yielding an overall average 5.5% mass loss from each monolith.

We then used ICP to confirm the composition of the leached Al-SS monoliths. The samples contained 18% Al on average, representing an Al mass loss of ~7%. The remainder is stainless steel. Optical microscopy of the monolith surface showed an increased surface roughness (Figure 2), creating a porous surface.

EDX mapping of the leached sample showed a homogeneous distribution of aluminium throughout the stainless steel with oxygen at the surface, suggesting the presence of surface aluminium oxide and/or hydroxide species (see SI). This was confirmed by X-ray photoelectron spectroscopy (XPS) measurements, which showed three contributing surface species: Aluminium hydroxides, aluminium oxides, and metallic aluminium (Figure 3).

To confirm the formation of porosity and calculate the corresponding surface area and pore volume, we analysed the Al-SS monoliths before and after leaching using N_2 sorption. For the hexagonal channel geometry, the pristine monolith had a surface area of 2830 mm^2, or 0.0013 m^2/g. Before leaching, N_2 sorption showed no porosity (see SI). Leaching yielded a porous surface with a BET surface area of 8 m^2/g. This may sound small compared to some porous catalysts, but it is an increase of the surface area by a factor of over 6000. The average BET pore volume was 0.006 cm^3/g and the average pore diameter was 3.04 nm. Moreover, the adsorption/desorption hysteresis confirmed the presence of micropores (Figure 4). Note that the measurement of such metallic surfaces requires extra careful sorption experiments due to the small areas.[20] We confirmed

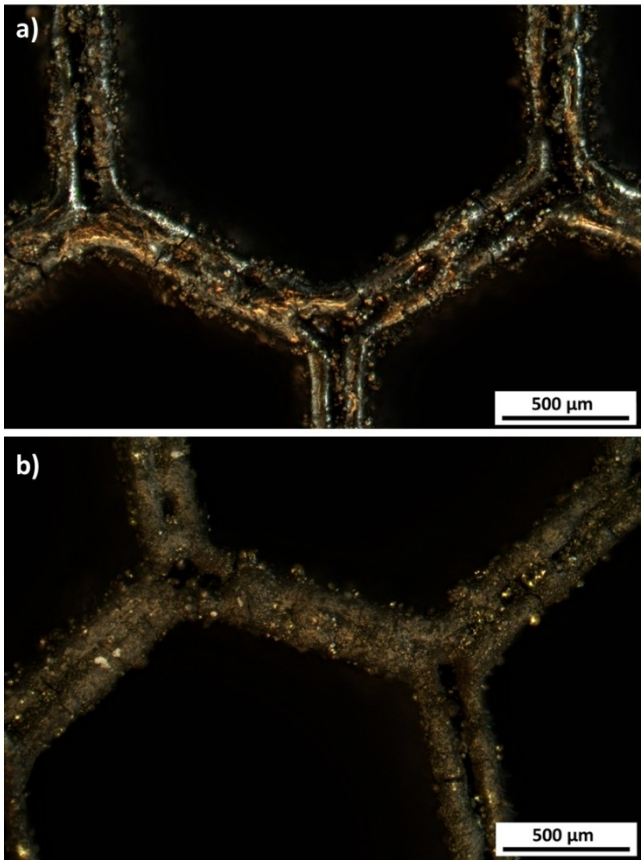

Figure 2. Optical microscopy images at magnification ×50 of a) a printed Al-SS monolith before pre-treatment or leaching and b) a monolith just after leaching.

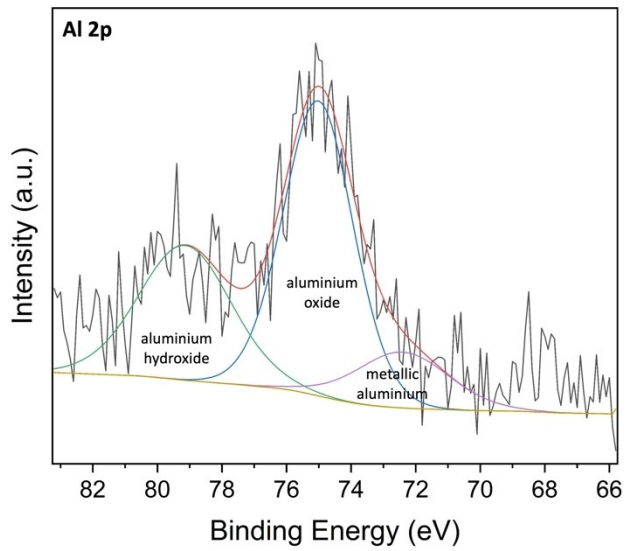

Figure 3. The aluminium 2p XPS scan of leached Al-SS sample.

the surface area and isotherm further using a series of control sorption measurements with SiO_2 as an internal standard (full isotherms and pore data included in the ESI).

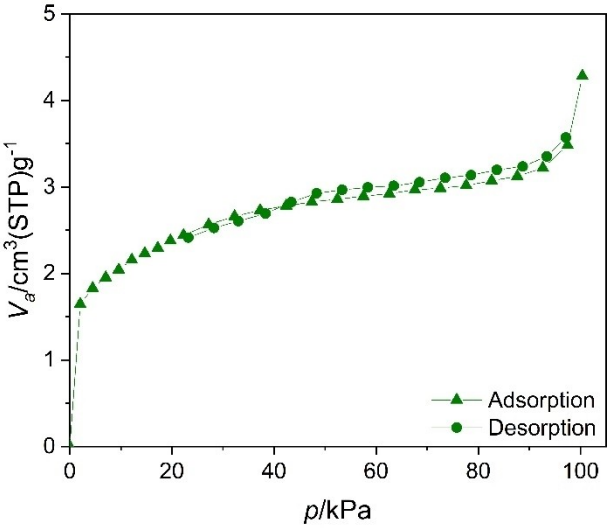

Figure 4. Nitrogen sorption isotherms of leached Al-SS monolith. The shape of the adsorption-desorption curve confirms the formation of micropores.

After optimising the leaching protocol, we tested the monoliths' performance in borohydride hydrolysis. Borohydrides react with water to form four equivalents of hydrogen gas and a metaborate by-product (Equation (1)). The spontaneous (background) reaction is slow and is inhibited by high pH.[21] By adding a catalyst, one can control the hydrogen release in high enough volumes for feeding a hydrogen fuel cell. The problem is that alkali borohydride hydrolysis incurs harsh conditions that cause catalyst failure in long-term applications. The vigorous formation of hydrogen bubbles at surface defects often damages the catalyst, limiting industrial use.

$NaBH_4$ has been a focus of research for mobile applications due to its high hydrogen density of 10.7 wt%.[22] However, its metaborate by-product is poorly soluble in water, limiting its practical application. Conversely, KBH_4, with a hydrogen density of 7.5 wt%, has a metaborate solubility that is five-fold higher than its sodium counterpart.[23–25] This makes KBH_4 a practical alternative (from the catalysis point of view, $NaBH_4$ and KBH_4 are interchangeable[14]).

We used a stabilised KBH_4 reaction solution (5% KBH_4, 5% KOH in water) for testing the activity and mechanical stability of our catalysts in both batch and continuous systems. Originally, we focused on cobalt-containing catalysts and tested the Al-SS supports only as blank controls. Surprisingly, we found that these "blanks" were active *even without any cobalt sites!* The reaction ran to completion, releasing the expected 100% yield of 4.3 L H_2 in less than 3 h, and outperforming our previously published Co-SS 3D printed catalysts (Figure 5, see SI for a detailed activity comparison).

Initially, we suspected that this activity comes from a stoichiometric reaction of Al^0 (that remained in the bulk) with hydroxide ions (see Equation (2)). However, a simple calculation shows that this is not the case. Even if all the aluminium in the sample would react with OH^- it would generate just 0.67 L of hydrogen, far less than the 4.3 L that we observed. Control

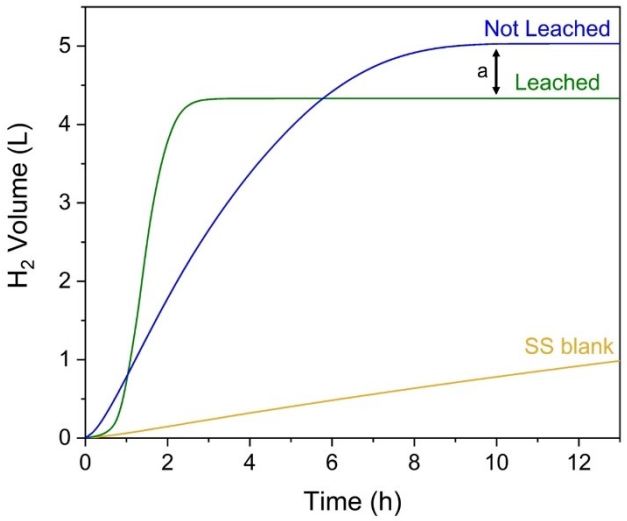

Figure 5. Total hydrogen volume generated in batch mode using leached (green curve) and unleached (blue curve) Al-SS catalysts. The yellow curve shows the background reaction with pure stainless steel for comparison. Measurements were made every second using two mass flow meters (MFMs) in series. All experiments were repeated in duplicate, with near-identical results.

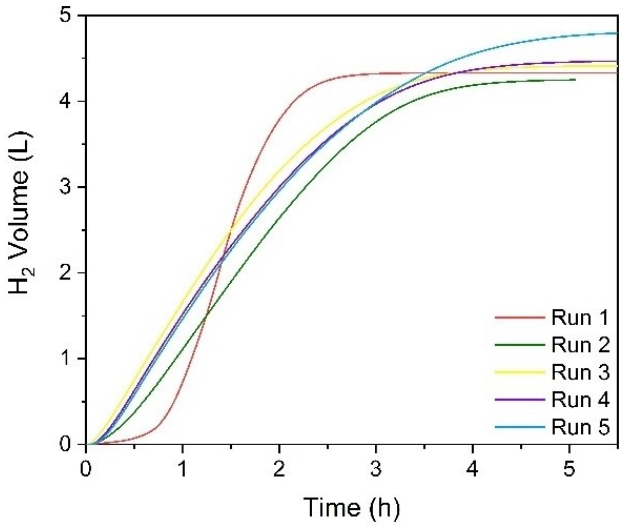

Figure 6. Multiple runs of a single leached Al-SS catalyst sample in batch mode. The hydrogen volume was measured every second using two MFMs in series. All experiments were repeated in duplicate, with near-identical results.

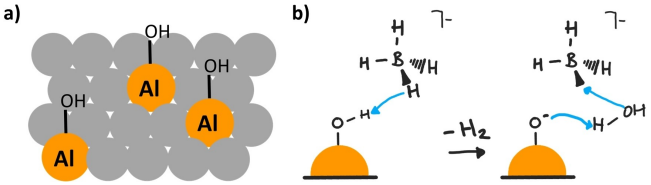

Scheme 1. Drawings of a) the active Al surface within SS and b) a proposed mechanism by which the Al could undergo catalysis for the borohydride hydrolysis.

experiments using an Al-SS monolith that had *not* been leached indeed show an additional H_2 release (Figure 5, blue curve, the additional hydrogen release is shown as 'a'). This exceeds the expected 100% yield from the borohydride hydrolysis of this batch size.[18,26–30] However, the reaction was much slower, and repeat runs using the same not-leached monolith did not show this additional release.

To confirm the lack of Al consumption in the leached Al-SS monolith further, we ran ICP analysis of the spent catalyst samples. The Al and Fe content was unchanged (18% and 54% respectively). Furthermore, unlike our first Co-SS samples,[15] the spent Al-SS monoliths showed no mass loss, even after extensive reactions and repeated experiments. From this analysis we can confidently say that the leached Al-SS monoliths are stable porous macrostructures that catalyse borohydride hydrolysis. This is remarkable, because these catalysts contain no PGMs nor CRMs. The catalytic active site is, in fact, aluminium-based.

One key difference between this catalyst and the Co-SS version is the induction period seen in the first 40 minutes. We attribute this induction period to mass-transfer limitations, caused by a combination of the porous catalyst and the viscous fuel solution.[31] The latter can be reduced by stirring, which also shortens the induction period, and *vice versa* (see SI for details).[32] The KOH, which is required for inhibiting the spontaneous hydrolysis of the borohydride, is the primary source of viscosity. When running multiple back-to-back reactions we observed the induction period only during the first run, as the pores need to be filled (Figure 6). This is a common trait in systems with mass transport limitations.[33]

There is no detailed published mechanism for aluminium-catalysed KBH_4 hydrolysis. Scheme 1a shows the active sites, which we believe to be Al-OH (they cannot be Al^0, as this would result in their consumption rather than catalysis). Scheme 1b shows a possible version of the first hydride abstraction step, known to be rate-determining in borohydride hydrolysis.[34] The Al-OH proton can react with a hydride of the BH_4^-. Then, a hydroxide from the surrounding water would attack the boron, forming the borohydride/metaborate intermediate. The proton from the water molecule would then transfer to the Al site, regenerating the Al-OH. The sequence would continue stepwise, until four molecules of hydrogen and a metaborate side product are formed. This pathway is analogous to the mechanism proposed by Demirci *et al.*, where boron centres in cobalt-polyborates would facilitate borohydride hydrolysis. In theory, the presence of other metal oxides from the stainless steel, such as chromium and nickel, could promote the catalysis of borohydride hydrolysis.[35–37] However, they are unlikely to be active centres in our case, *cf.* the lack of activity of the stainless steel blanks (Figure 5).

Following the batch system optimisation, we ran continuous long-term testing (still on lab scale; a detailed description of the continuous setup is published elsewhere[15]). To test the catalysts extended stability of the monolith, we tested a leached sample in our continuous reactor system over 100 h. Here we pumped a feed solution of 5% KBH_4 and 5% KOH through the active porous Al-SS monolith at a rate of 0.8 mL/min for 100 h.

Figure 7 shows that the monolith maintains its activity throughout the test, with an average hydrogen release > 50 mL/min.

We compared this catalyst to our previous 3D-printed one, using a monolith of 1.5 wt% cobalt embedded in stainless steel (Co-SS, no aluminium).[15] Figure 8 shows that the Al-SS monolith clearly outperforms the Co-SS on both activity and chemical and mechanical stability. The Co-SS lost mass, while Al-SS did not. Furthermore, when the Al-SS was transferred after 100 h in the continuous reactor to the batch reactor it maintained its high reaction rate and the reaction ran to completion, with no poisoning of the surface (see SI for details).

As a final comparison, we also prepared the porous leached monoliths containing both 20% aluminium and 1.5% cobalt (Co–Al-SS). Nitrogen sorption studies showed the same porosity for these cobalt-containing monoliths as for the cobalt-free ones (Figure 9, cf. with Figure 4) with a similar BET surface area of 7.4 m^2/g. Batch and continuous tests using the same feed solution of 5% KBH_4 and 5% KOH showed comparable activity and stability in hydrogen generation. We conclude that the presence of aluminium overshadows any effects of the cobalt in this case.

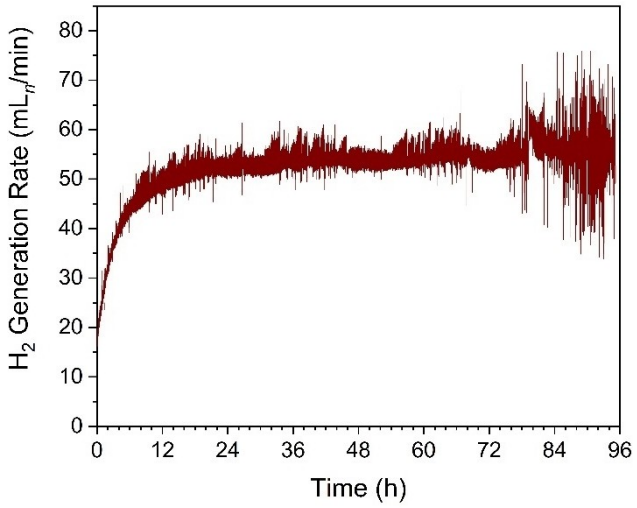

Figure 7. Hydrogen generation rate of one leached Al-SS monolith tested in a continuous reactor with 5% KBH_4 and 5% KOH in water. H_2 generation rate was measured every second by two MFMs in series.

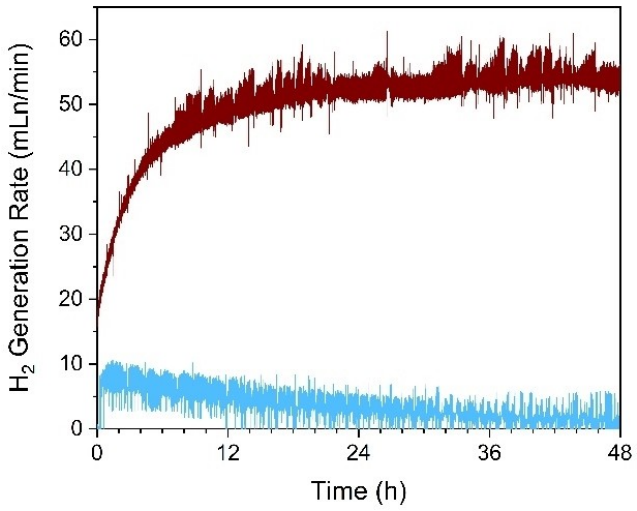

Figure 8. Comparison of H_2 generation rates of the previously reported 1.5 wt% Co-SS monolith (blue) vs. leached Al-SS monolith (red) of this work. Reactions were run in the same continuous reaction system under identical conditions. For the Co-SS catalysts, signal artefacts caused by large bubble formation (ca. 300 points) have been removed for clarity, while still leaving 170,000 points shown. The full dataset and a detailed explanation of these artefacts is included in the SI.

To quantify our work's contribution to sustainability, we first compared the performance of the Al-SS catalyst with that of other published catalysts (Table 1). We chose the exposure time of the catalyst to the borohydride solution (durability) as the comparison metric, since the focus on activity can be misleading in this case. There are many catalysts that show high activity in borohydride hydrolysis over a short period and/or at low feed concentrations. However, few studies give the actual amounts of hydrogen generated per measurable unit of catalyst over several hours or more. There are two reasons for this: First, running reactions for many hours costs time and efforts, and second, the catalysts tend to deactivate. However, for real-world applications, long-term mechanical and chemical stability are a must. On this metric we see that our Al-SS catalysts outperform both our own Co-SS and Co-chitosan catalysts as well as many other examples.

Other important sustainability metrics are resource abundance and cost-effectiveness. The ingot prices of the aluminium and stainless steel raw materials, at the time of writing, were 2.11 $/kg and 0.79 $/kg respectively. For commercial powders with the correct particle size and shape, this cost jumps to 800 $/kg and 75 $/kg, respectively. The Al-SS catalyst would therefore cost 220 $/kg in raw materials, or $0.48 per catalyst monolith. Considering the long-term activity and stability, this is not expensive, and it would be even cheaper on larger scale. Note that this catalyst contains no noble metals (PGM-free) and indeed no critical raw materials (CRM-free). Both stainless steel

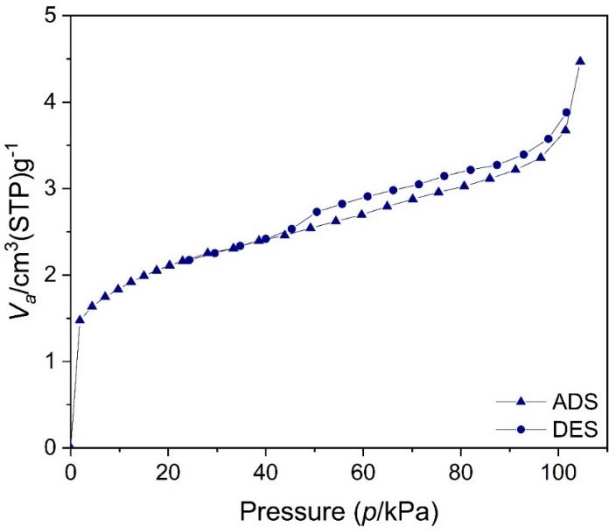

Figure 9. N_2 adsorption isotherm of 1.5% Co-Al-SS. This shows that the leached catalyst containing cobalt is microporous after leaching. Without leaching there is no porosity (see SI for details).

Table 1. Comparing catalyst durability across studies.

Cat.	React.	Feed conc. (wt%)	Hydroxide (wt%)	Cat. exposure time	Ref
Al-SS	KBH_4	5	5 (KOH)	96 h	This work
Co-Al-SS	KBH_4	5	5 (KOH)	96 h	This work
Co-SS	KBH_4	5	5 (KOH)	48 h	[15]
Co chitosan	KBH_4	5	5 (KOH)	48 h	[14]
Co-B-O	$NaBH_4$	0.00012	–	6 h	[38]
Co-B/SS	$NaBH_4$	19	4.5 (NaOH)	9 h	[12]
CoB/NiF	$NaBH_4$	9–28	4.5 (NaOH)	1.2 h	[39]
Ni–Al alloy	$NaBH_4$	10	5 (NaOH)	20 h	[40]
Co-W-B/NiF	$NaBH_4$	20	5 (NaOH)	1.6 h	[41]
Co-Ni-P/Cu	$NaBH_4$	10	10 (NaOH)	60 h	[42]
Intrazeolite Co(0) nanoclusters	$NaBH_4$	0.56	10 (NaOH)	100 h	[43]
Co-B/Pd	$NaBH_4$	20	4 (NaOH)	1.2	[44]
Co-P	$NaBH_4$	10	1 (NaOH)	100 h	[45]

and aluminium are fully recyclable, reducing the consumption of new resources for catalyst synthesis.[46] This is a significant advancement from previous research.

Finally, the catalyst preparation procedure also has green chemistry benefits. 3D printing is a low-waste process that requires no additional solvents or water. Any excess powder can be reused after a simple sieving step. The acid pre-washing and base leaching steps require only minimal amounts of aqueous acid and base solutions. Moreover, no carbon-containing materials are used during the catalyst synthesis or its application.

Conclusions

By combining selective laser melting with acid/base leaching we have successfully created macroscopic microporous all-metallic objects. This proof-of-concept confirms that we can generate porosity in metal catalysts and still maintain structural integrity under harsh reaction conditions. The micropores enable easy access of small molecules and ions to the catalytic active sites. A surprise bonus is the unexpected activity of aluminium in this configuration for borohydride hydrolysis. The combination of versatile 3D-printed macrostructures, abundant raw materials and high chemical reactivity and stability opens exciting opportunities for this new family of catalysts in hydrogen generation and other applications. We hope that this paper will encourage more research groups to use these methods, so that everyone can benefit from a steep learning curve.

Experimental Section

Materials and Instrumentation

Stainless steel (316 L, max. particle size 63 μm) was purchased from AP&C (a GE additive company) and cobalt powder (max. particle size 45 μm) was purchased from Sigma Aldrich. Aluminium powder was sourced from R&G Faserverbundwerkstoffe GmbH and then sieved to remove particles over 63 μm. Sieving was done using a Russell AMProLab sieve under N_2 flow with a 63 μm aperture mesh. Pre-processing of CAD files into slices was done using Autodesk Netfabb for toolpath generation. 3D printing was done using a Concept Laser Mlab R printer (fibre laser) with the Selective Laser Melting (SLM) technique onto a stainless steel plate in an inert atmosphere ($<$ 1% O_2). A Sodick SLC400 G with a brass electrode wire of 250 μm (Megacut® Plus Ø 0.25 mm) was used to remove the pieces from the plate using the 'coarse' cutting parameter. A Delphin-X Observer was used with a sCMEX-20 camera to take optical microscopy images. Processing of images was done using ImageFocusAlpha software. N_2 sorption isotherms were measured on a BelSorp-maxII instrument at 77 K with pretreatment done at 200 °C. The samples were pre-treated overnight in vacuum at 200 °C. Microwave digestion was done using an Anton Paar Multiwave Pro 50 Hz and ICP-OES measurements were done on an Agilent 5800 VDV Spectrometer. Bronkhorst EL-Flow Prestige mass flow meters were set up in series (200 mL_n/min and 2 L_n/min) to measure the H_2 flow rate every second for both batch and continuous systems, and Bronkhorst Flowsuite software was used to collect the data. Origin 2018 was used for all data processing.

General Procedure for Catalyst Synthesis Using 3D Printing

Al powder was sieved in bulk to remove all particles over 63 μm. Stainless steel powder and the sieved aluminium were

mixed in a weight percentage of 80 and 20 wt%, respectively, to make a 450 g powder batch (360 g stainless steel powder and 90 g aluminium powder). The powders were mixed manually. This powder supply batch was then loaded into the 3D printer were the CAD file and printing parameters (Table 2) were uploaded. 3D printing of monoliths was done six pieces at a time on a stainless steel base plate. The samples were removed from the platform by means of Wire EDM using a brass wire. Then, they were put in an acid solution (60 wt% H_2SO_4, 5 wt% HNO_3, 35 wt% H_2O) for 16 h. Afterwards they were washed with H_2O until all acid was removed. Leaching was then done at 90 °C in a 7 M NaOH solution for 16 h, using a reflux condenser to ensure water vapour retention. After leaching, the samples were washed with H_2O until all hydroxide was removed, then left to dry in air overnight.

Hydrogen Generation (Batch Reaction)

50 mL of H_2O was pre-heated to 65 °C and KOH (5%, 2.5 g, 0.9 M) was added. In a three-neck round bottom flask, KBH_4 (5%, 2.5 g, 0.9 M) was added with a stir bar. The catalyst was hung through one neck of the flask and sealed with a septum. A dropping funnel with the KOH solution was connected to another neck, whilst the last neck was connected to a cold trap. This setup was put into an oil bath at 65 °C with stirring at 250 rpm. The system was flushed with air before the KOH was added to the KBH_4 with the catalyst submerged in solution, at which point the H_2 flow rate was measured.

Hydrogen Generation (Continuous Reaction)

Continuous reactions were performed at 65 °C with a liquid flow rate of 0.8 mL/min. A room temperature solution of KOH (5%, 0.89 M) and KBH_4 (5%, 0.93 M) was pumped into the continuous reactor and heated in the oven. Gas produced passed through a phase separator and a water bubbler before passing through two mass flow meters in series (2 L_n/min and 200 mL_n/min).

Table 2. Parameters of the 3D printer used for the synthesis of the catalysts.

Parameter	Value
Laser power (surface area exposure)	90.25 W
Laser power (contour exposure)	60 W
Laser speed (surface area exposure)	600 mm/s
Laser speed (contour exposure)	450 mm/s
Layer height	25 μm
Spot size	50 μm
Hatch distance	83 μm
Max. particle size of powder	63 μm
Atmosphere	N_2 ($O_2 < 0.3$%)

ICP

Microwave digestion was done in a solution of nitric acid, hydrogen peroxide and water. Higher concentrated elements were diluted once (Cr, Mo, Ni) or twice (Al, Fe) in $HNO_3 + H_2O_2 + H_2O$ by Factor 100 before microwave digestion. All elemental concentrations are presented independent of the dilution. The ICP-OES analysis was performed on at least three emission wavelengths for all analysed elements. The reported concentrations are averaged from two independent measurements, where validation criteria were < 10% standard deviation from the mean value. The axial or radial view of plasma was used depending on the concentration range.

Acknowledgments

This work was funded by the "Austrian COMET-Program" (project InTribology1, no. 872176) via the Austrian Research Promotion Agency (FFG) and the federal states of Niederösterreich and Vorarlberg and has been carried out within the "Excellence Centre of Tribology" (AC2T research GmbH).

Conflict of Interests

The authors declare no conflict of interest.

Data Availability Statement

The data that support the findings of this study are available from the corresponding author upon reasonable request.

Keywords: PGM-free · Additive manufacturing · Hydrogen generation · Catalyst degradation · CRM-free

[1] P. K. Pathak, A. K. Yadav, S. Padmanaban, *Int. J. Hydrogen Energy* **2023**, *48*, 9921–9927.
[2] G. Rothenberg, *Sustain. Chem. Climate Action* **2023**, *2*, 100012.
[3] L. Depraiter, S. Goutte, *Resour. Policy* **2023**, *86*, 104137.
[4] C. O'Connor, T. Alexandrova, *Minerals* **2021**, *11*, 54.
[5] L. Talens Peiró, G. Villalba Méndez, R. U. Ayres, *JOM* **2013**, *65*, 986–996.
[6] C. Banza Lubaba Nkulu, L. Casas, V. Haufroid, T. De Putter, N. D. Saenen, T. Kayembe-Kitenge, P. Musa Obadia, D. Kyanika Wa Mukoma, J.-M. Lunda Ilunga, T. S. Nawrot, O. Luboya Numbi, E. Smolders, B. Nemery, *Nat. Sustain.* **2018**, *1*, 495–504.
[7] T. Dutta, K.-H. Kim, M. Uchimiya, E. E. Kwon, B.-H. Jeon, A. Deep, S.-T. Yun, *Environ. Res.* **2016**, *150*, 182–190.
[8] J. Teubler, S. Kiefer, C. Liedtke, *Resources* **2018**, *7*, 49.
[9] A. Ajanovic, M. Sayer, R. Haas, *Int. J. Hydrogen Energy* **2022**, *47*, 24136–24154.
[10] U. B. Demirci, O. Akdim, J. Andrieux, J. Hannauer, R. Chamoun, P. Miele, *Fuel Cells* **2010**, *10*, 335–350.
[11] O. Akdim, U. B. Demirci, P. Miele, *Int. J. Hydrogen Energy* **2011**, *36*, 13669–13675.
[12] G. M. Arzac, D. Hufschmidt, M. C. Jiménez De Haro, A. Fernández, B. Sarmiento, M. A. Jiménez, M. M. Jiménez, *Int. J. Hydrogen Energy* **2012**, *37*, 14373–14381.
[13] S. Eugénio, U. B. Demirci, T. M. Silva, M. J. Carmezim, M. F. Montemor, *Int. J. Hydrogen Energy* **2016**, *41*, 8438–8448.

[14] F. Pope, J. Jonk, M. Fowler, P. C. M. Laan, N. J. Geels, L. Drangai, V. Gitis, G. Rothenberg, *Green Chem.* **2023**, *25*, 5727–5734.
[15] F. Pope, M. Fowler, D. Giesen, L. Drangai, G. Rothenberg, *Chem. Eng. Technol.* **2024**, *47*, 932–939.
[16] R. Murray, *Method of Producing Finely-Divided Nickel* **1927**, US1628190 A.
[17] N. T. Aboulkhair, M. Simonelli, L. Parry, I. Ashcroft, C. Tuck, R. Hague, *Prog. Mater. Sci.* **2019**, *106*, 100578.
[18] J. Macanás, L. Soler, A. M. Candela, M. Muñoz, J. Casado, *Energy* **2011**, *36*, 2493–2501.
[19] D. Karbalaei Saleh, H. Abdollahi, M. Noaparast, A. Fallah Nosratabad, *Clay Miner.* **2019**, *54*, 209–217.
[20] E.-J. Ras, M. J. Louwerse, M. C. Mittelmeijer-Hazeleger, G. Rothenberg, *Phys. Chem. Chem. Phys.* **2013**, *15*, 4436–4443.
[21] H. I. Schlesinger, H. C. Brown, A. E. Finholt, J. R. Gilbreath, H. R. Hoekstra, E. K. Hyde, *J. Am. Chem. Soc.* **1953**, *75*, 215–219.
[22] L. Laversenne, C. Goutaudier, R. Chiriac, C. Sigala, B. Bonnetot, *J. Therm. Anal. Calorim.* **2008**, *94*, 785–790.
[23] N. P. Nies, R. W. Hulbert, *J. Chem. Eng. Data* **1967**, *12*, 303–313.
[24] P. Toledano, *Compt. Rend. Acad. Sci.* **1962**, *254*, 2348–2350.
[25] O. Krol, J. Andrieux, J. J. Counioux, R. Tenu, C. Goutaudier, *in XXXV JEEP – 35th Conference on Phase Equilibria*, EDP Sciences, Annecy, France **2009**, 00023.
[26] H. Zou, S. Chen, Z. Zhao, W. Lin, *J. Alloys Compd.* **2013**, *578*, 380–384.
[27] D. Belitskus, *J. Electrochem. Soc.* **1970**, *117*, 1097–1099.
[28] H.-B. Dai, G.-L. Ma, X.-D. Kang, P. Wang, *Catal. Today* **2011**, *170*, 50–55.
[29] L. Soler, J. Macanás, M. Muñoz, J. Casado, *Int. J. Hydrogen Energy* **2007**, *32*, 4702–4710.
[30] D.-W. Zhuang, J.-J. Zhang, H.-B. Dai, P. Wang, *Int. J. Hydrogen Energy* **2013**, *38*, 10845–10850.
[31] L. B. Hitchcock, J. S. Mcilhenny, *Ind. Eng. Chem.* **1935**, *27*, 461–466.
[32] F. Pope, N. I. Watson, A. Deblais, G. Rothenberg, *ChemPhysChem* **2022**, *23*, e202200428.
[33] D. Y. Murzin, T. Salmi, D. Y. Murzin, T. Salmi, *in Catalytic Kinetics*, Elsevier, Amsterdam **2016**, 2nd ed., 589–664.
[34] Y. Zhou, C. Fang, Y. Fang, F. Zhu, H. Liu, H. Ge, *Int. J. Hydrogen Energy* **2016**, *41*, 22668–22676.
[35] R. Fernandes, N. Patel, A. Miotello, *Appl. Catal. B Environ.* **2009**, *92*, 68–74.
[36] N. Patel, R. Fernandes, A. Miotello, *J. Catal.* **2010**, *271*, 315–324.
[37] Y. Xia, Y. Pei, Y. Wang, F. Li, Q. Li, *Fuel* **2023**, *331*, 125733.
[38] A. M. Ozerova, V. I. Simagina, O. V. Komova, O. V. Netskina, G. V. Odegova, O. A. Bulavchenko, N. A. Rudina, *J. Alloys Compd.* **2012**, *513*, 266–272.
[39] G. M. Arzac, A. Fernández, A. Justo, B. Sarmiento, M. A. Jiménez, M. M. Jiménez, *J. Power Sources* **2011**, *196*, 4388–4395.
[40] Y.-J. Lee, Y.-S. Lee, H. A. Shin, Y. S. Jo, H. Jeong, H. Sohn, C. W. Yoon, Y. Kim, K.-B. Kim, S. W. Nam, *J. Alloys Compd.* **2020**, *843*, 155759.
[41] H. B. Dai, Y. Liang, P. Wang, X. D. Yao, T. Rufford, M. Lu, H. M. Cheng, *Int. J. Hydrogen Energy* **2008**, *33*, 4405–4412.
[42] D.-R. Kim, K.-W. Cho, Y.-I. Choi, C.-J. Park, *Int. J. Hydrogen Energy* **2009**, *34*, 2622–2630.
[43] M. Rakap, S. Özkar, *App. Catal. B: Environ.* **2009**, *91*, 21–29.
[44] J. Liang, Y. Li, Y. Huang, J. Yang, H. Tang, Z. Wei, P. K. Shen, *Int. J. Hydrogen Energy* **2008**, *33*, 4048–4054.
[45] K. Eom, H. Kwon, *Int. J. Hydrogen Energy* **2010**, *35*, 5220–5226.
[46] Directorate-General for Internal Market, European CommissionPublications Office of The European Union 2023: Industry, Entrepreneurship and SMEsM. Grohol, C. Veeh, Study on the Critical Raw Materials for the EUFinal Report 2023, https://data.europa.eu/doi/10.2873/725585

Manuscript received: June 13, 2024
Revised manuscript received: August 29, 2024
Version of record online: October 29, 2024